JPE 16-1-25

http://dx.doi.org/10.6113/JPE.2016.16.1.238
ISSN(Print): 1598-2092 / ISSN(Online): 2093-4718

State Estimation Technique for VRLA Batteries for Automotive Applications

Van Huan Duong*, Ngoc Tham Tran*, Woojin Choi†, and Dae-Wook Kim**

*,†Dept. of Electrical Engineering, Soongsil University, Seoul, Korea
**Dept. of Economics, Soongsil University, Seoul, Korea

Abstract

The state-of-charge (SOC) and state-of-health (SOH) estimation of batteries play important roles in managing batteries for automotive applications. However, an accurate state estimation of a battery is difficult to achieve because of certain factors, such as measurement noise, highly nonlinear characteristics, strong hysteresis phenomenon, and diffusion effect of batteries. In certain vehicular applications, such as idle stop–start systems (ISSs), significant errors in SOC/SOH estimation may lead to a failure in restarting a combustion engine after the shut-off period of the engine when the vehicle is at rest, such as at a traffic light. In this paper, a dual extended Kalman filter algorithm with a dynamic equivalent circuit model of a lead–acid battery is proposed to deal with this problem. The proposed algorithm adopts a battery model by taking into account the hysteresis phenomenon, diffusion effect, and parameter variations for accurate state estimations of the battery. The validity of the proposed algorithm is verified through experiments by using an absorbed glass mat valve-regulated lead–acid battery and a battery sensor cable for commercial ISS vehicles.

Key words: Dual Extended Kalman Filter (DEFK), Hysteresis Effect, Diffusion Effect, Idle Start–Stop (ISS) System, State-of-Charge (SOC)/State-of-Health (SOH) Estimation

I. INTRODUCTION

In most countries, global warming has become a significant issue that requires urgent action in terms of decreasing greenhouse gas emissions, particularly in the automotive sector. Electric vehicles (EVs), such as battery EVs, hybrid EVs (HEVs), and plug-in HEVs, are promising solutions that can considerably lower the amount of greenhouse gas emissions and achieve better fuel efficiency than conventional vehicles. Electric cars will undoubtedly play an increasingly large role in many countries in the decades ahead as energy independence and environmental concerns intensify. However, EVs are estimated to gain only a modest ground up to 2020 [1]. Gasoline- and diesel-powered vehicles are improving faster than expected and will continue to dominate the global landscape. In addition, carmakers are trying to meet future emission targets mainly through improvements in internal combustion engines (ICEs). Idle start–stop (ISS) systems are becoming increasingly prevalent in ICEs because of their ability to reduce emissions and fuel consumption in a cost-effective manner. An ISS system is an easy and low-cost technology that enables an ICE to power off automatically when the car is stopped and to restart upon demand. As a result, the ICE undergoes far more starting events, and the behavior of the ICE during startup becomes more critical. In this kind of vehicle, valve-regulated lead–acid (VRLA) batteries are often employed because of their maintenance-free characteristics and higher resistance to shock and vibrations. Batteries operate under intense conditions because of their frequent charge and discharge cycles and cranking; therefore, accurately estimating the state of charge (SOC) and state of health (SOH) of batteries is crucial to avoid failures of restarting the engine after being shut down. Moreover, battery state information is essential to enhance the efficiency of battery energy utilization, lengthen the lifetime of the battery, and prevent permanent damage to the battery.

Several methods of estimating the SOC and SOH of a battery have been proposed by using coulomb counting, artificial neutron networks (ANNs), fuzzy logic (FL), and extended Kalman filters (EKFs) [2]-[10]. The coulomb

Manuscript received May 19, 2015; accepted Sep. 5, 2015
Recommended for publication by Associate Editor Jonghoon Kim.
†Corresponding Author: cwj777@ssu.ac.kr
Tel: +82-2-820-0652, Fax: +82-2-817-7961, Soongsil University
*Dept. of Electrical Engineering, Soongsil University, Korea
**Dept. of Economics, Soongsil University, Korea

counting method can be simply implemented by integrating the battery current over time [11]. However, the reliability of SOC estimation cannot be maintained when errors accumulate over the operation time and when the initial value of the SOC is wrong. The ANNs and FL approaches can estimate the SOC of a battery with an arbitrary initial SOC value. However, these methods are relatively expensive to implement and require the training data of the battery [12]. The EKF is a popularly accepted tool that provides a theoretically well-designed and time-proven method to filter the measurements of the system input and output to produce an intelligent estimation of the dynamic state of a system [13]-[15]. The dual EKF (DEKF) algorithm is a combination of two EKFs, in which the SOC is estimated by the first EKF, and the capacity is estimated by the second EKF [16]. The main advantage of this method is that it can provide reliable estimation results while the battery is in operation. As a result, the DEKF algorithm is preferred among the abovementioned methods. However, because the estimation accuracy depends mainly on the adoption of a comprehensive and well-parameterized battery model, robust SOC/SOH estimation is possible only when the model is accurate enough.

Although precise modeling of a battery plays an important role in estimating SOC/SOH accurately, it is a complicated and challenging task because VRLA batteries show nonlinear characteristics, and various factors should be considered. For example, the parameters of the equivalent circuit model of a battery depend mainly on operating conditions, such as the SOC of the battery, charge/discharge current, and temperature [17]. The hysteresis phenomenon is a history-dependent characteristic caused by internal chemical processes that cause difficulties in estimating the SOC, particularly when the battery state turns over from a partial charge or discharge [18], [19]. In addition, the diffusion effect, which has a relatively long time constant, has to be considered to improve the estimation accuracy.

In this paper, an accurate SOC/SOH estimation method using DEKF for absorbed glass mat (AGM) type VRLA batteries is proposed. A practical battery model that considers hysteresis and diffusion phenomenon is introduced. The hysteresis effect is modeled by calculating the normalized integration of the charge throughput during a partial cycle, and the diffusion phenomenon is considered by reconstructing the open circuit voltage (OCV) decay depending on the rest time. The size of the state matrix calculation for the Kalman filter operation can be significantly reduced by incorporating the diffusion effect into the OCV. In addition, the dependency of the battery parameters on various internal and external conditions, such as SOC, temperature, and charge/discharge current and their combinations, are considered based on pretest results from the battery. All the test methods for modeling hysteresis, diffusion, and parameter variations are detailed in the following sections. The proposed algorithm is implemented in a battery sensor cable (BSC) with an ARM7 microprocessor and validated through experimental results.

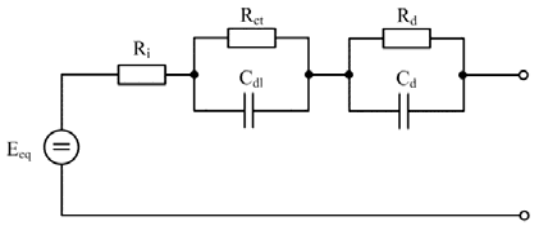

Fig. 1. Popular model of a lead–acid battery.

II. Pretest Methods for Modeling an AGM VRLA Battery

A. Popular Model of a Lead–Acid Battery

Fig. 1 shows a popular model of a lead–acid battery that consists of a voltage source, a series resistor, and two sets of parallel resistor–capacitor circuits. In the figure, E_{eq} represents the equilibrium voltage of the battery, and R_i represents the resistance of the contacts, the inter cell connections, and the electrolyte. R_{ct} and C_{dl} are the charge-transfer resistor and electric double-layer capacitor, respectively, which represent the charge transfer reaction; R_d and C_d are the diffusion resistor and diffusion capacitor, respectively, which represent the diffusion phenomenon caused by the grade of the concentration of the electrolyte near the electrode [20]. The phenomenon causes a second overvoltage on the electrode potential called "diffusion overvoltage." This model is suitable for describing the dynamic behavior of a VRLA battery. However, the model is unsuitable for a Kalman filter operation because using the model would lead to computational overkill.

A lithium–ion battery, a simple method that uses a single average OCV–SOC relationship, can be employed because the hysteresis phenomenon is negligible. Hence, SOC estimation can be achieved with high precision without considering the hysteresis effect [22]-[24]. However, modeling an AGM VRLA battery is not feasible without considering the hysteresis phenomenon because a large error can result from estimating the OCV of a battery during a dynamic operation. In this study, the hysteresis is modeled by approximating it with a parallelogram. Then, the hysteresis factor is introduced to track the voltage variations caused by hysteresis depending on the charge throughput.

All the parameters of the model vary sensitively depending on the SOC, temperature, and charge/discharge current, as previously mentioned. Thus, the parameter variations have to be modeled carefully. To model the parameter variations, comprehensive pretests have to be conducted by using current pulse tests. All the pretests required to model an AGM VRLA battery are described in the following sections.

B. Pretests to Develop the Proposed AGM VRLA Battery Model

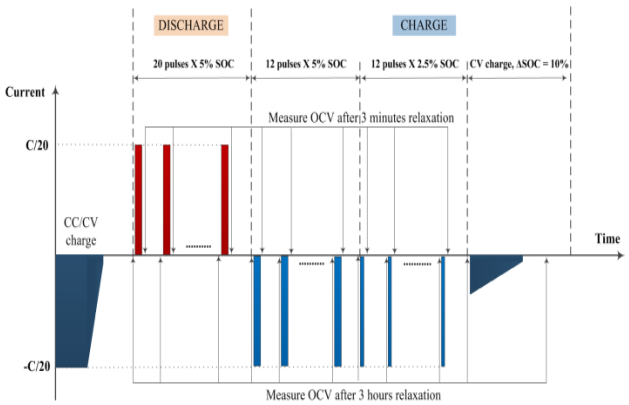

Fig. 2. Full cycle test procedure to obtain the OCV–SOC relationship of the AGM VRLA battery.

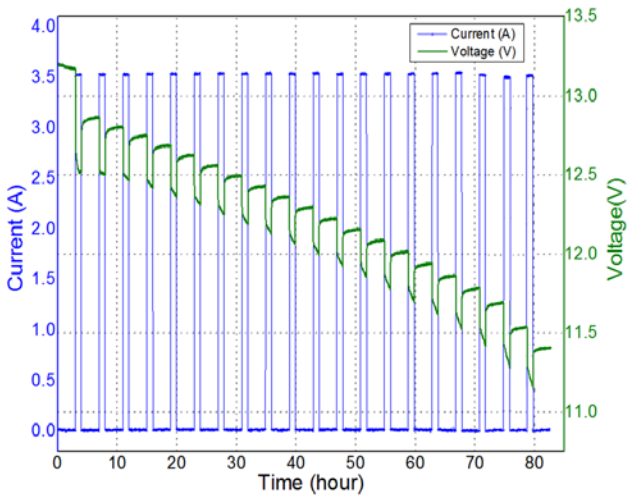

Fig. 3. Measured current and voltage waveforms of the AGM VRLA battery during the discharge at 25 °C.

In this section, a comprehensive explanation for the pretests required to model an AGM VRLA battery is described in detail. The following three kinds of pretests must be conducted to model the battery:

1) Full cycle test to derive the relationship between the SOC and the OCV and to extract the diffusion overvoltage:
2) Partial cycle test to model the hysteresis loop; and
3) Variable current pulse test to model the parameter variations.

An AGM VRLA battery (Solite AGM70L – DIN, 12 V, 70 Ah) is used for the tests, and all the tests are conducted in a constant temperature chamber. The battery is connected to a bipolar DC power supply (NF BP4610), and a program created in LabView 11.0 is used to perform the tests automatically. The charge/discharge cycle profile created in LabView is transmitted to the external control port of the bipolar DC power supply via the D/A converter of the data acquisition board (NI PCI DAQ 6154), and the bipolar power supply charges and discharges the battery exactly as commanded. A sensing circuit for the voltage and current is

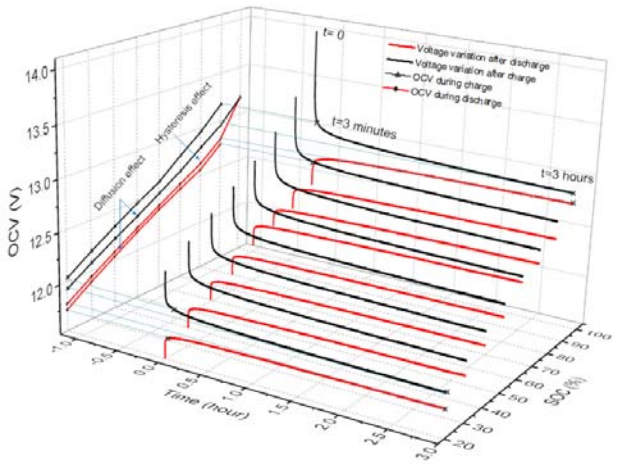

Fig. 4. OCV–SOC relationship at each SOC obtained from the full cycle test at 25 °C.

used to measure the terminal voltage and the current of the battery and the data acquisition board record them.

1) Full Cycle Test to Derive the Relationship between the SOC and the OCV: To derive the OCV–SOC relationship, a charge/discharge test that uses variable current pulses is performed, as shown in Fig. 2. The magnitude and duration of the current pulse are C/20 and 1 h, respectively. Hence, each pulse is equivalent to 5% of the actual capacity. Twenty of these discharge current pulses are applied to the fully charged battery to fully discharge the battery. Then, the battery is charged again with the same current pulse until it reaches 60% of the SOC. Then, the duration of the current pulse is reduced to 0.5 h, and the current pulse is applied to the battery until it reaches 90% of the SOC. At this point, the battery is fully charged by a constant voltage charge until it reaches 100% of the SOC. The relaxation time between each pulse is 3 h, thereby ensuring that the measurement of the true OCV is possible. Fig. 3 shows the measured voltage and current of the battery obtained through the discharge test at 25 °C. The charge/discharge current and the terminal voltage of the battery are recorded at every second in a host computer through a data acquisition board. The full cycle test procedure is then repeated at -18, 0, and 45 °C The measured terminal voltages of the battery at 25 °C after charge and discharge at different SOC values are presented using three-dimensional plots in Fig. 4. The OCV–SOC curve with a 3 min relaxation and a 3 h relaxation can be obtained as the projections of the battery voltage at 3 min and 3 h after the charge/discharge pulse current are removed. The OCV during charging is higher than that during discharging at the same SOC because of the hysteresis effect [21].

On the basis of the full cycle test results, the measured OCV curves at 25 °C with a 3-min relaxation and a 3 h relaxation and the difference between them are depicted in Fig. 5. Each of the OCV–SOC curves can be modeled by a fifth-order polynomial function and represented as follows:

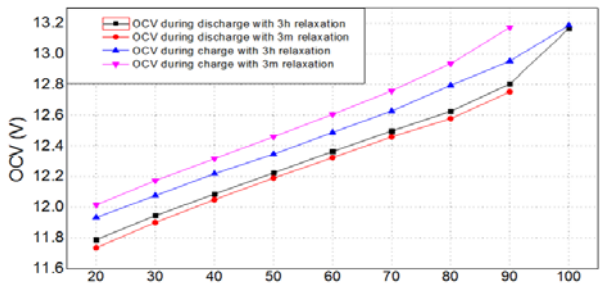

(a)

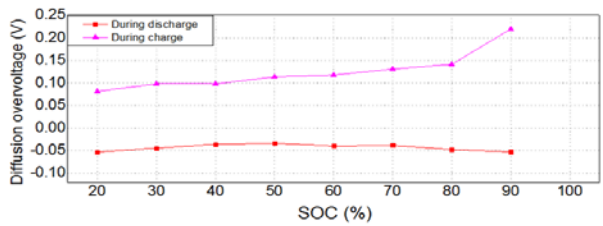

(b)

Fig. 5. (a) OCV–SOC curve with 3-min and 3-g relaxation at 25 °C. (b) OCV difference between 3-min and 3-h relaxation curves.

TABLE I
COEFFICIENTS OF THE POLYNOMIAL EQUATIONS FOR EACH OCV–SOC CURVE AT 25 °C

OCV-SOC	a_0	a_1	a_2	a_3	a_4	a_5
OCV_{c3h}	11.449	3.279	- 6.783	11.510	-9.719	3.442
OCV_{c3m}	11.486	3.805	- 8.984	16.349	-14.593	5.301
OCV_{d3h}	11.323	3.215	- 6.334	10.827	-9.016	2.853
OCV_{d3m}	11.314	2.565	- 2.889	3.396	-1.915	0.329

$$\mathrm{OCV}(SOC)=a_0+a_1SOC+a_2SOC^2+a_3SOC^3+a_4SOC^4+a_5SOC^5. \quad (1)$$

The coefficients of the polynomial equations are listed in Table I. The measured curves at -18, 0, and 45°C are also modeled with Equ. (1), and the OCV value at a certain temperature can be determined by using an interpolation technique that can construct new data based on the range of the obtained data of the OCV from the full cycle tests [25].

The OCV lies between the OCV curve with the 3 min relaxation and the 3 h relaxation after the charge transfer overvoltage vanishes; thus, it can be modeled by using diffusion factor ζ, which can be calculated with time constant τ_d of the R_d–C_d circuit as

$$\zeta(t_{rest})=\begin{cases}1 & \text{if} \quad t_{rest}<180s\\ \exp\left(\dfrac{180-t_{rest}}{\tau_d}\right) & \text{if} \quad t_{rest}\geq 180s\end{cases}. \quad (2)$$

During the charge, the OCV can be reconstructed by using diffusion factor ζ as follows:

$$\begin{cases}OCV_c(SOC,\zeta)=OCV_{c3h}(SOC)+\zeta V_d(SOC)\\ V_d(SOC)=OCV_{c3m}(SOC)-OCV_{c3h}(SOC)\end{cases}. \quad (3)$$

Thus, during the charging, the OCV can be calculated as Equ. (4) depending on the relaxation time, and the OCV can also be calculated in the same manner as follows:

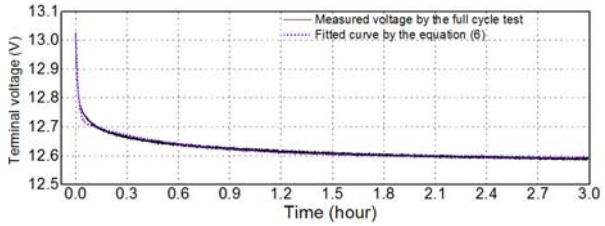

(a)

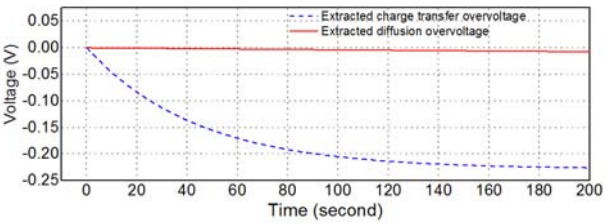

(b)

Fig. 6. Voltage variation after a charge current pulse at 65% of SOC at 25 °C. (a) Measured voltage and fitted results with the model in Fig. 1. (b) Extracted charge transfer overvoltage and diffusion overvoltage.

$$OCV_c(SOC,\zeta)=(1-\zeta)OCV_{c3h}(SOC)+\zeta OCV_{c3m}(SOC) \quad (4)$$

and

$$OCV_d(SOC,\zeta)=(1-\zeta)OCV_{d3h}(SOC)+\zeta OCV_{d3m}(SOC). \quad (5)$$

As mentioned in Section II A, the diffusion overvoltage needs to be extracted and merged into the OCV to simplify the battery model. Fig. 6(a) shows the terminal voltage variation of the battery voltage after the C/20 charge current is removed at 65% of the SOC. The voltage decay can be divided into two parts by the charge transfer overvoltage and the diffusion overvoltage, except for the immediate voltage drop, because of resistance R_i. The charge transfer overvoltage is caused by R_{ct}-C_{dl} in the battery model and is dominant in the transient voltage in the first 3 min and vanishes afterwards. Thus, the voltage decay after 3 min can be considered diffusion overvoltage that has a relatively long time constant. The terminal voltage of the battery can be represented by Equ. (6), and the parameters can be extracted simply by using the curve fitting

$$y=y_0+A_1(1-\exp(\frac{-t_{rest}}{\tau_1}))+A_2(1-\exp(\frac{-t_{rest}}{\tau_2})), \quad (6)$$

where y_0 is the dc offset, t_{rest} is the relaxation time of the battery after charging or discharging, and A_1 and A_2 are the coefficients of the first and the second exponential terms, respectively. τ_1 and τ_2 represent the time constants of the R_{ct}–C_{dl} and R_d–C_d circuit, respectively. This test is repeated at each SOC, and the average value of τ_2 is used to calculate diffusion factor ζ in Equ. (2).

In these results, the extracted charge transfer overvoltage and diffusion overvoltage can be drawn as Fig. 6(b), and the battery model can be simplified by merging the diffusion overvoltage into equilibrium voltage E_{eq}. E_{eq} is reconstructed to a voltage source, which varies not only with the SOC but

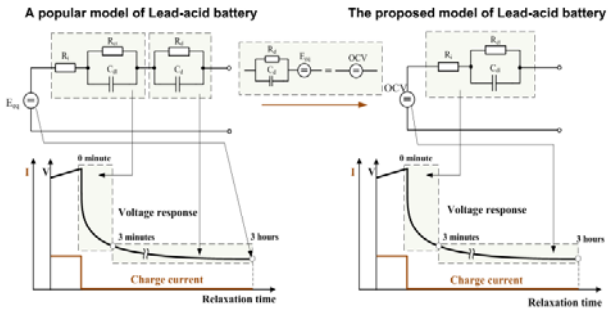

Fig. 7. Proposed battery model with the reconstructed OCV.

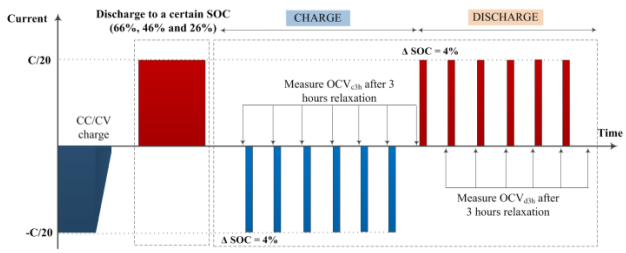

Fig. 8. Partial cycle test procedure for the hysteresis loop modeling.

also with the relaxation time, as illustrated in Fig. 7 [26].

2) Partial Cycle Test to Model the Hysteresis Loop: Obtaining the voltage trajectory when hysteresis occurs is necessary because the hysteresis loop can be modeled by a parallelogram [17], [19], [21]. The partial cycle test is conducted to obtain information about the hysteresis loop. The current pulses illustrated in Fig. 8 are used for the partial cycle tests. In this case, a current pulse equivalent to 4% of the actual capacity of the battery is used for the tests. At first, a fully charged battery is rested for 3 h. The battery is discharged continuously to 66% of the SOC and charged to 90% of the SOC by using six current pulses. Then, the battery is discharged again to 66% of the SOC with the same current pulses, as depicted in Fig. 8. This test is repeated at three different SOC ranges to derive the average value of the parameters to model the hysteresis with a parallelogram.

In these results, the hysteresis loop can be modeled with the partial cycle test results by a parallelogram, as shown in Fig. 9. The actual OCV during charging and discharging lies somewhere in between the 3 h relaxation charge and discharge curves depending on the charge throughput [18].

Thus, the transition of the OCV can be empirically reconstructed by introducing a hysteresis model. Hysteresis factor α is introduced to model the movement of the OCV between the lower boundary curve (3 h relaxation discharge curve OCV_{d3h}) and the upper boundary curve (3 h relaxation charge curve OCV_{c3h}) during a partial charge/discharge cycle. The OCV reconstruction considering the hysteresis effect can be performed by

$$\begin{cases} OCV(SOC,\alpha) = OCV_{d3h}(SOC) + \alpha V_{hys}(SOC) \\ V_{hys}(SOC) = OCV_{c3h}(SOC) - OCV_{d3h}(SOC) \end{cases}. \quad (7)$$

Equ. (7) can be simplified as follows:

$$OCV(SOC,\alpha) = (1-\alpha)OCV_{d3h}(SOC) + \alpha OCV_{c3h}(SOC) \quad (8)$$

The empirical equation for hysteresis factor α corresponding to the charge throughput can be described by Equ. (9), as shown in Fig. 9(a):

$$\alpha = \alpha_1 + \alpha_2 . \quad (9)$$

Hysteresis factor α varies at a different rate according to the charge throughput; thus, the values of α_1 and α_2 must be calculated by Equs. (10) and (11), and updated with the charge throughput at each time index k

$$\alpha_{1,k} = \alpha_{1,k-1} + \frac{K}{\Delta SOC_{1\max}}\Delta SOC, \text{ for} \begin{cases} 0 \le \alpha_{1,k} \le K \\ \Delta SOC \le \Delta SOC_{1\max} \end{cases}; \quad (10)$$

$$\alpha_{2,k} = \alpha_{2,k-1} + \frac{1-K}{\Delta SOC_{2\max}}\Delta SOC, \text{ for} \begin{cases} 0 \le \alpha_{2,k} \le 1-K \\ \Delta SOC \le \Delta SOC_{2\max} \end{cases}. \quad (11)$$

For instance, when a battery is being charged, α_1 is calculated first until the charge throughput reaches 4%, and then α_2 is calculated until the charge throughput reaches 24%. When the charge throughput exceeds 24%, the hysteresis effect disappears, and the OCV follows the boundary curve. Similarly, when the battery is being discharged, α_1 is decreased to 0 first, and then α_2 is decreased. The charge throughput can be calculated by

$$\Delta SOC = \frac{\Delta t.I}{3600.C_b} \quad (12)$$

where C_b (Ah) is the capacity of the battery, and Δt is the sampling time. The *K* value, ΔSOC_{1max}, and ΔSOC_{2max} can be simply extracted by using least square fitting with the test data and a parallelogram, as shown in Fig. 9(a).

Fig. 9(b) shows three hysteresis test results performed at different SOC values, and the results are used to calculate hysteresis factor α , which exhibits small differences at each SOC value. Table II shows the variation of the *K* values at three different SOC ranges for the partial cycle tests. The average value of *K* can be used to simplify the hysteresis voltage calculation because the values of *K* are almost the same regardless of the SOC range.

3) Variable Current Pulse Tests to Model Parameter Variations: DEKF is a popular technique that can provide a powerful and intelligent solution for the online state estimation of a battery [16]. However, the accuracy of DEKF depends significantly on the accuracy of the parameter values in the battery model. As previously mentioned, battery parameters vary according to the operating conditions of the battery, such as the SOC, temperature, and charge/discharge current value [27], [28]. Thus, the parameter variations of the battery model have to be modeled carefully and taken into account for the DEKF operation. To model the parameter variations of the battery, variable charge/discharge current pulses, which have different amplitudes (C/1, C/2, C/5, C/10, C/20, and C/40 [A]) and durations (1, 2, 5, 12, 24, and 51 [min]), are applied to the battery, as shown in Fig. 10.

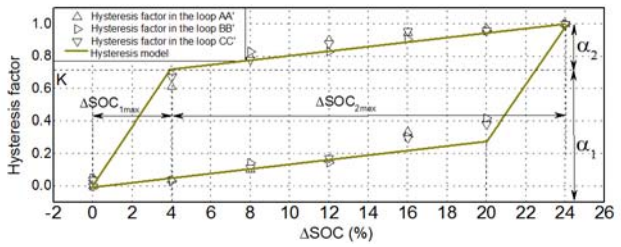

(a)

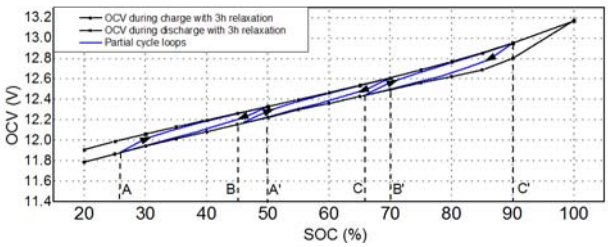

(b)

Fig. 9. (a) Modeling of the hysteresis loop with the partial cycle test results by a parallelogram. (b) Partial cycle tests performed at three different SOC ranges.

TABLE II

K VALUES OBTAINED AT THREE DIFFERENT SOC RANGES BY THE PARTIAL CYCLE TESTS

SOC range for the partial cycle tests	*K*
A–A` (66%–90%)	0.74
B–B` (46%–70%)	0.76
C–C` (26%–50%)	0.75

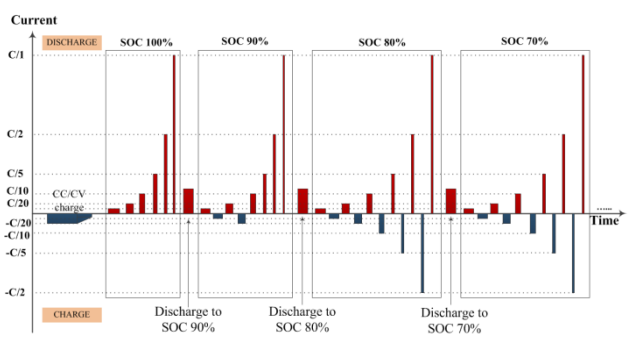

Fig. 10. Variable current pulse tests to model the parameter variation.

Tests are conducted at each SOC level (10% SOC step from 100% to 40%) to obtain information about the parameter variations. Thereafter, the tests are repeated at different temperatures (-18, 0, 25, and 45 °C) to investigate the temperature dependency of the battery parameters. After all the data are collected, the curve fitting technique is used to extract battery parameters, such as R_i, R_{ct}, and C_{dl}. As a result, the parameter variations caused by changes in the SOC, temperature, and charge/discharge current value can be modeled.

Fig. 11 shows the variation of charge transfer resistance R_{ct} at different temperatures. R_{ct} varies exponentially depending

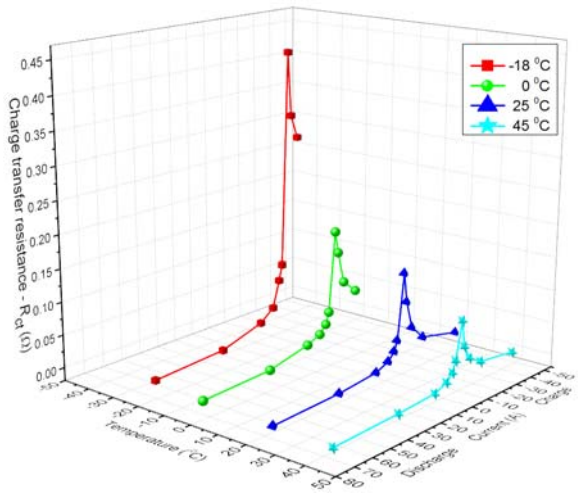

Fig. 11. Variation of R_{ct} according to the charge/discharge current at each temperature.

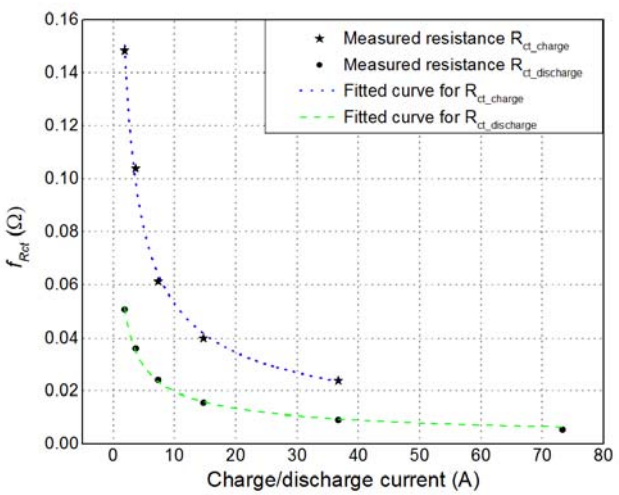

Fig. 12. Variation of R_{ct} depending on the charge/discharge current at 25 °C fitted by the exponential functions.

on the current values. Fig. 12 shows the variation of R_{ct} depending on the charge/discharge current at 25 °C, and R_{ct} is fitted by the exponential function as

$$f_{R_{ct}}(I) = m_{R_{ct}} . I^{-n_{R_{ct}}} . \quad (13)$$

The coefficients of Equ. (13), namely, m_{Rct} and n_{Rct}, are given in Table III.

Fig. 13 shows the variation of R_{ct} depending on the SOC of the battery. In this case, the normalized value of R_{ct} with respect to its value at SOC = 70% depending on the SOC is drawn and fitted by the second-order polynomial equation in

$$g_{R_{ct}}(SOC) = a_{R_{ct}} . SOC^2 + b_{R_{ct}} . SOC + c_{R_{ct}} . \quad (14)$$

The coefficients of Equ. (14), namely, a_{Rct}, b_{Rct}, and c_{Rct}, are given in Table III.

Fig. 14 shows the variation of R_{ct} depending on temperature. In this case, the normalized value of R_{ct} with respect to its value at 25 °C depending on the temperature is drawn and fitted by the exponential function in

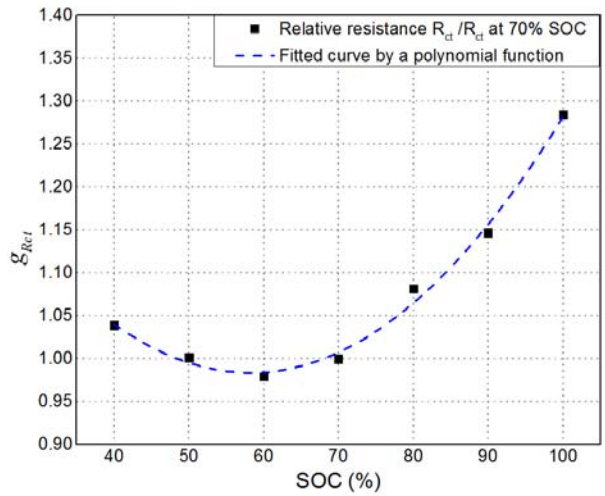

Fig. 13. Variation of the normalized R_{ct} value with respect to its value at 70% SOC depending on the SOC fitted by a second-order polynomial function.

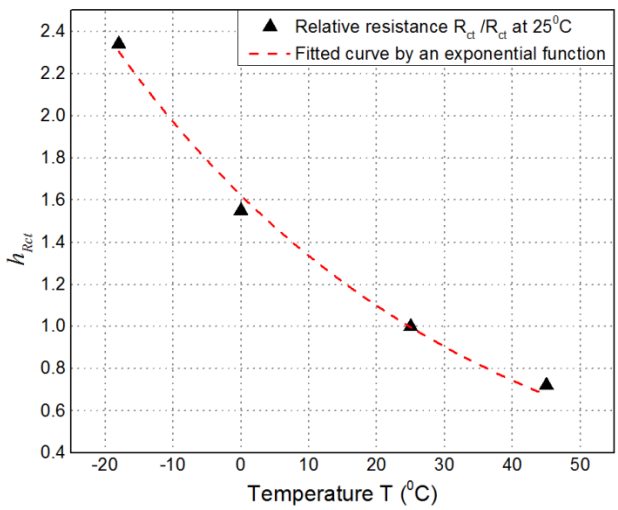

Fig. 14. Variation of the normalized R_{ct} value with respect to its value at 25 °C fitted by an exponential function.

TABLE III
COEFFICIENTS OF EQUATIONS (13), (14), AND (15)

Function	Factors
$f_{Rct}(I)$	m_{Rct} = 0.05462; n_{Rct} = 0.4762 during discharging m_{Rct} = 0.21951; n_{Rct} = 0.6242 during charging
$g_{Rct}(SOC)$	$a_{Rct} = 4.1964e^{-4}$; b_{Rct} = -0.5312; c_{Rct} = 2.26625
$h_{Rct}(T)$	m'_{Rct} = 1.5838; n'_{Rct} = 0.02

$$h_{R_{ct}}(T) = m'_{R_{ct}}.e^{-n'_{R_{ct}}.T}. \quad (15)$$

The coefficients of Equ. (15), namely, $m'_{Rct,}$ and n'_{Rct}, are given in Table III.

As investigated in [29], the parameters can be adjusted according to the SOC, temperature, and charge/discharge current value by using the following:

$$R_{ct} = f_{R_{ct}}(I).g_{R_{ct}}(SOC).h_{R_{ct}}(T). \quad (16)$$

The parameters of the battery model in the DEKF can now be updated by using Equ. (16) on a real-time basis, thereby maintaining the accuracy of the battery model.

III. STATE ESTIMATION TECHNIQUE OF AN AGM VRLA BATTERY BY USING THE DEKF ALGORITHM

A. DEKF Algorithm for SOC/SOH Estimation

The SOC indicates the relative level of charge presently held by a battery, whereas the SOH refers to the general decline in battery performance with respect to usage or aging. Therefore, estimating the SOC and SOH of a battery is important to predict the remaining useful energy and the remaining service life of the battery. In this paper, the DEFK approach is used to estimate the SOC and SOH of a battery. The DEFK process essentially combines two EKFs that run in parallel, where one is the state filter for estimating the SOC, and the other is the weighting filter for estimating the capacity [16, 30]. At each time interval, the state filter uses the priori value of the weight filter and vice versa. The step-by-step calculation procedure is summarized as follows.

The nonlinear state–space model can be represented as

$$\mathbf{x}_{k+1} = \mathrm{f}(\mathbf{x}_k, \mathbf{u}_k, \boldsymbol{\theta}_k) + \mathbf{w}_k \quad , \quad \boldsymbol{\theta}_{k+1} = \boldsymbol{\theta}_k + \mathbf{r}_k \quad (17)$$

and

$$\mathbf{y}_k = \mathrm{g}(\mathbf{x}_k, \mathbf{u}_k, \boldsymbol{\theta}_k) + \mathbf{v}_k \,, \; \mathbf{d}_k = \mathrm{g}(\mathbf{x}_k, \mathbf{u}_k, \boldsymbol{\theta}_k) + \mathbf{e}_k \,, \quad (18)$$

where $\mathbf{x}_k$ is the state vector of the battery model, $\boldsymbol{\theta}_k$ is the time varying battery capacity, $\mathbf{u}_k$ is the exogenous input, $\mathbf{y}_k$ is the system output, and $\mathbf{w}_k$, $\mathbf{v}_k$, $\mathbf{r}_k$, and $\mathbf{e}_k$ are independent Gaussian noise processes with covariance matrices $\mathbf{Q}_k^x$, $\mathbf{R}_k^x$, $\mathbf{Q}_k^\theta$, and $\mathbf{R}_k^\theta$, respectively. $\mathrm{f}(\cdot,\cdot,\cdot)$ represents a nonlinear transition matrix function, and $\mathrm{g}(\cdot,\cdot,\cdot)$ represents a nonlinear measurement matrix function.

The computing procedure for the DEFK can be summarized as follows [16].

Step 1: Initializing at k=0.

$$\begin{aligned} \hat{\boldsymbol{\theta}}_0^+ &= \mathbf{E}\left[\mathbf{x}_0\right], \hat{\mathbf{P}}_{\theta,0}^+ = \mathbf{E}\left[\left(\boldsymbol{\theta}_0 - \hat{\boldsymbol{\theta}}_0^+\right)\left(\boldsymbol{\theta}_0 - \hat{\boldsymbol{\theta}}_0^+\right)^T\right], \\ \hat{\mathbf{x}}_0^+ &= \mathbf{E}\left[\mathbf{x}_0\right], \hat{\mathbf{P}}_{\tilde{x},0}^+ = \mathbf{E}\left[\left(\mathbf{x}_0 - \hat{\mathbf{x}}_0^+\right)\left(\mathbf{x}_0 - \hat{\mathbf{x}}_0^+\right)^T\right] \end{aligned} \quad (19)$$

where E[.] is the statistical expectation operator.

Step 2: Approximating the nonlinear functions.

$$\begin{cases} \mathbf{F}_{k-1} = \left.\dfrac{\partial \mathrm{f}(\mathbf{x}_{k-1}, \mathbf{u}_{k-1}, \hat{\boldsymbol{\theta}}_k^-)}{\partial \mathbf{x}_{k-1}}\right|_{x_{k-1}=\hat{x}_{k-1}^+} \\ \mathbf{G}_k^x = \left.\dfrac{\partial \mathrm{g}\left(\mathbf{x}_k, \mathbf{u}_k, \hat{\boldsymbol{\theta}}_k^-\right)}{\partial \mathbf{x}_k}\right|_{x_k=\hat{x}_k^-}, \quad \mathbf{G}_k^\theta = \left.\dfrac{d\,\mathrm{g}\left(\mathbf{x}_k, \mathbf{u}_k, \hat{\boldsymbol{\theta}}_k^-\right)}{d\theta}\right|_{\theta=\hat{\theta}_k^-} \end{cases} \quad (20)$$

Step 3: Updating the time for each filter.

State filter:

$$\hat{\mathbf{x}}_k^- = \mathrm{f}(\hat{\mathbf{x}}_{k-1}^+, \mathbf{u}_{k-1}, \hat{\boldsymbol{\theta}}_k^-) \tag{21}$$

$$\mathbf{P}_{x,k}^- = \mathbf{F}_{k-1}\mathbf{P}_{x,k-1}^+\mathbf{F}_{k-1}^T + \mathbf{Q}_k^x \tag{22}$$

Weight filter:

$$\hat{\boldsymbol{\theta}}_k^- = \hat{\boldsymbol{\theta}}_{k-1}^+ \tag{23}$$

$$\mathbf{P}_{\theta,k}^- = \mathbf{P}_{\theta,k-1}^+ + \mathbf{Q}_k^\theta \tag{24}$$

Step 4: Updating the measurement for each filter.

State filter:

$$\mathbf{K}_k^x = \mathbf{P}_{x,k}^-\left(\mathbf{G}_k^x\right)^T\left[\mathbf{G}_k^x\mathbf{P}_k^-\left(\mathbf{G}_k^x\right)^T + \mathbf{R}_k^x\right]^{-1} \tag{25}$$

$$\hat{\mathbf{x}}_k^+ = \hat{\mathbf{x}}_k^- + \mathbf{K}_k^x\left[y_k - \mathrm{g}\left(\hat{\mathbf{x}}_k^-, \mathbf{u}_k, \hat{\boldsymbol{\theta}}_k^-\right)\right] \tag{26}$$

$$\mathbf{P}_{x,k}^+ = \left(\mathbf{I} - \mathbf{K}_k^x\mathbf{G}_k^x\right)\mathbf{P}_{x,k}^- \tag{27}$$

Weight filter:

$$\mathbf{K}_k^\theta = \mathbf{P}_{\theta,k}^-\left(\mathbf{G}_k^\theta\right)^T\left[\mathbf{G}_k^\theta\mathbf{P}_k^-\left(\mathbf{G}_k^\theta\right)^T + \mathbf{R}_k^\theta\right]^{-1} \tag{28}$$

$$\hat{\boldsymbol{\theta}}_k^+ = \hat{\boldsymbol{\theta}}_k^- + \mathbf{K}_k^\theta\left[y_k - \mathrm{g}\left(\hat{\mathbf{x}}_k^-, \mathbf{u}_k, \hat{\boldsymbol{\theta}}_k^-\right)\right] \tag{29}$$

$$\mathbf{P}_{\theta,k}^+ = \left(\mathbf{I} - \mathbf{K}_k^\theta\mathbf{G}_k^\theta\right)\mathbf{P}_{\theta,k}^- \tag{30}$$

B. SOC/SOH Estimation using the DEKF Algorithm

The state space equation for the proposed battery model in Fig. 7 in a discrete form can be represented as

$$\mathbf{x}_{k+1} = \begin{pmatrix} SOC_{k+1} \\ V_{Cdl,k+1} \end{pmatrix} = \begin{pmatrix} 1 & 0 \\ 0 & 1 - \dfrac{\Delta t}{R_{ct,k}C_{dl,k}} \end{pmatrix}\begin{pmatrix} SOC_k \\ V_{Cdl,k} \end{pmatrix} + \begin{pmatrix} -\dfrac{\Delta t}{C_{b,k}} & \dfrac{\Delta t}{C_{dl,k}} \end{pmatrix}^T I_k + w_k \tag{31}$$

and

$$\theta_k = \left[C_{b,k}\right]. \tag{32}$$

The terminal voltage of the battery model can be represented by using a nonlinear function as follows:

$$\mathbf{y}_k = \mathrm{OCV}\left(SOC_k, \zeta_k, \alpha_k\right) - V_{Cdl,k} - R_i I_k + v_k. \tag{33}$$

The OCV value at each time index k can be reconstructed by using Equs. (4), (5), and (6)

$$\begin{aligned} OCV\left(SOC_k, \zeta_k, \alpha_k\right) = {} & (1-\alpha_k)\begin{bmatrix} (1-\zeta_k)OCV_{d3h}(SOC_k) \\ +\zeta_k OCV_{d3m}(SOC_k) \end{bmatrix} \\ & +\alpha_k\begin{bmatrix} (1-\zeta_k)OCV_{c3h}(SOC_k) \\ +\zeta_k OCV_{c3m}(SOC_k) \end{bmatrix} \end{aligned}. \tag{34}$$

Equation (34) can be rewritten in a compact form as

$$OCV\left(SOC_k, \zeta_k, \alpha_k\right) = \sum_{i=0}^{5} a_{i,k}SOC_k^i \tag{35}$$

where

$$a_{i,k} = (1-\alpha_k)\left[\zeta_k a_{d3m_{i,k}} + (1-\zeta_k)a_{d3h_{i,k}}\right] + \alpha_k\left[\zeta_k a_{c3m_{i,k}} + (1-\zeta_k)a_{c3h_{i,k}}\right].$$

While the state equation in Equ. (36), as shown below, does not require an approximation, the nonlinear measurement function g(.,.) requires an approximation because the OCV–SOC relationship is nonlinear:

$$\mathbf{F}_{k-1} = \begin{pmatrix} 1 & 0 \\ 0 & 1 - \dfrac{\Delta t}{R_{ct}C_{dl}} \end{pmatrix}. \tag{36}$$

Thus, the Taylor series approximation described in the following equations is used for linearization:

$$\mathbf{G}_k^x = \begin{bmatrix} \dfrac{\partial OCV}{\partial \hat{z}_k^-} & -\dfrac{\partial V_{Cdl\,k}}{\partial V_{Cdl\,k}} \end{bmatrix} = \begin{bmatrix} \displaystyle\sum_{i=0}^{4}(i+1)a_{i,k}\left(z_k^-\right)^i & -1 \end{bmatrix} \tag{37}$$

and

$$\mathbf{G}_k^\theta = \frac{dg\left(\hat{x}_k^-, u_k, \theta\right)}{d\theta} = \frac{\partial g\left(\hat{x}_k^-, u_k, \theta\right)}{\partial \theta} + \frac{\partial g\left(\hat{x}_k^-, u_k, \theta\right)}{\partial \hat{x}_k^-}\frac{d\hat{x}_k^-}{d\theta}, \tag{38}$$

where

$$\frac{d\hat{x}_k^-}{d\theta} = \frac{\partial f\left(\hat{x}_{k-1}^+, u_{k-1}, \theta\right)}{\partial \theta} + \frac{\partial f\left(\hat{x}_{k-1}^+, u_{k-1}, \theta\right)}{\partial \hat{x}_k^+}\frac{d\hat{x}_{k-1}^+}{d\theta}$$

$$\frac{d\hat{x}_{k-1}^+}{d\theta} = \frac{d\hat{x}_{k-1}^-}{d\theta} - L_{k-1}^x\frac{dg\left(\hat{x}_{k-1}^-, u_{k-1}, \theta\right)}{d\theta}.$$

The partial derivatives are computed at each time step, whereas the total derivatives are computed recursively with zero as initial values.

IV. Experimental Verification of the Proposed Algorithm

To verify the validity of the proposed estimation algorithm by using the DEKF, the proposed algorithm is tested with an AGM VRLA battery. A Solite AGM70L-DIN (12 V, 70 Ah) battery is used to verify the proposed method. The algorithm is implemented by using C language in the ARM7 TDMI microprocessor integrated into the BSC for the ISS EV application, as shown in Fig. 15.

The battery is fully charged up to 100% of the SOC and then discharged to 50% of the SOC. Thereafter, the battery is charged and discharged repeatedly with different amounts of charge, and eventually, charging is stopped at 78% of the SOC. In this experiment, coulomb counting is considered the reference value of the estimation for the performance comparison.

The DEKF algorithm initially uses the coulomb counting method to estimate the SOC value. Then, the error between the measured terminal voltage and the estimated terminal voltage is used to correct the priori SOC value that is calculated by the coulomb counting method in a real-time update step. In this way, the DEKF can solve the problem of determining the initial SOC and eliminate the accumulated error caused by coulomb counting over long-term operation. Fifty percent of the SOC is used as an initial value instead of 100% of the SOC to verify that the DEKF converges to the true SOC value with a wrong initial SOC value. As shown in Fig. 16, the SOC estimation error at the beginning is 50%. After 1.5 h of operation, the SOC error is reduced to less than

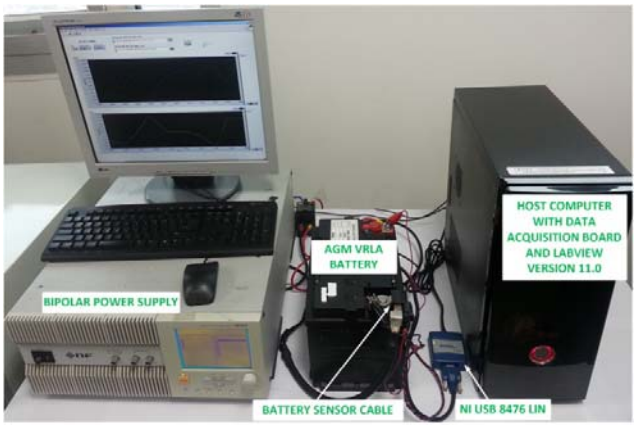

Fig. 15. Implementation of the proposed algorithm in the ARM7TDMI microprocessor of the battery sensor cable.

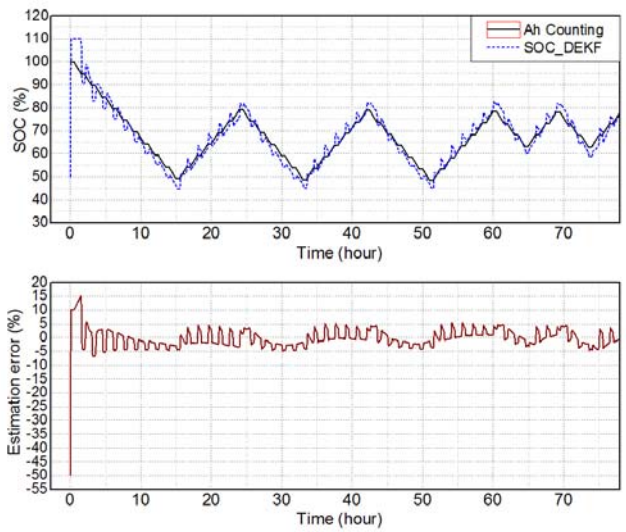

Fig. 16. SOC estimation results and errors of the proposed algorithm.

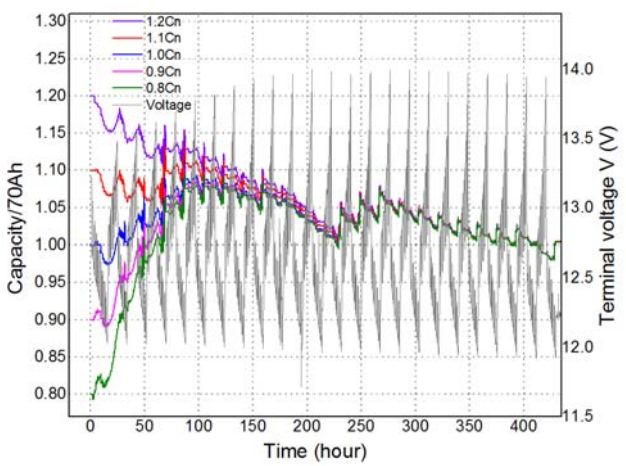

Fig. 17. Capacity estimation results with the different initial capacity values.

15%, and afterward, it remains less than 5%. The error becomes larger when the battery changes its state from charged to discharged, and vice versa, because of the strong hysteresis effect.

However, the error in the SOC estimation is still less than 5% over the entire test period. On the basis of these results, the proposed battery model, which includes the hysteresis, diffusion effect, and parameter variations, is good enough to reproduce the electric behavior accurately to provide reliable SOC estimation.

To guarantee the operation of the DEKF algorithm for estimating battery capacity, a pulse current cycle test that comprises a sequence of discharge pulses and relaxation, followed by a sequence of charge pulses and relaxation, is conducted. The terminal voltage and the current of the battery are recorded by the host computer and data acquisition board every second during the 450 h of the test. The proposed algorithm is also coded by LabView and tested with the recorded data. Capacity estimation results with a true initial value (0.98 Cn = 68.6 Ah) and wrong initial values, which are smaller and larger than the true value, are shown in Fig. 17. Five different initial capacity values (0.8, 0.9, 1.0, 1.1, and 1.2 Cn) are used in this test. As shown in Fig. 17, the real capacity of the battery can be estimated successfully by the proposed algorithm with less than 5% error after approximately 300 h in all cases. Results demonstrate the performance of the proposed algorithm in predicting the SOH of the battery; the proposed algorithm is determined to be suitable for ISS EV applications.

V. Conclusion

In this paper, a novel technique for estimating the SOC/SOH of AGM VRLA batteries based on the DEKF algorithm has been proposed, and its performance has been verified by experiments with an AGM VRLA battery. The battery model is simplified by reconstructing the OCV, considering the diffusion and hysteresis effects of the battery for the light computation of the Kalman filter. The parameter variations of the battery model according to the SOC, current, and temperature have been modeled by using pretest results with the battery and applied to the model during operation in a real-time basis. The observed error of the SOC and SOH estimation is less than 5%. The proposed method can be used in any kind of battery management system for vehicle and energy storage applications.

References

[1] X. Mosquet, M. Devineni, T. Mezger, H. Zablit, A. Dinger, G. Sticher, M. Gerrits, and M. Russo, "Poweing Autos to 2020, The Era of the Electric Car?," *The Boston Consulting Group*, Jul. 2011.

[2] E. Leksono, I. N. Haq, M. Iqbal, F. X. N. Soelami, and I. N. Merthayasa, "State of charge (SoC) estimation on LiFePO4 battery module using Coulomb counting methods with modified Peukert," in *Rural Information & Communication Technology and Electric-Vehicle Technology (rICT &*

ICeV-T), 2013 Joint International Conference on, pp. 1-4, 2013.
[3] M. Shahriari and M. Farrokhi, "Online state-of-health estimation of VRLA batteries using state of charge," *IEEE Trans. Ind. Electron.*, Vol. 60, No. 1, pp. 191-202, Jan. 2013.
[4] H.-T. Lin, T.-J. Liang, and S.-M. Chen, "Estimation of battery state of health using probabilistic neural network," *IEEE Trans. Ind. Informat.*, Vol. 9, No. 2, pp. 679-685, May 2013.
[5] R. Feng, S. Zhao, and X. Lu, "On-line estimation of Dynamic State-of-Charge for lead acid battery based on fuzzy logic," in *Measurement, Information and Control (ICMIC), 2013 International Conference on*, pp. 447-451, 2013.
[6] C. Zheng, Y. Fu, and C. C. Mi, "State of charge estimation of lithium-ion batteries in electric drive vehicles using extended Kalman filtering," *IEEE Trans. Veh. Technol.*, Vol. 62, No. 3, pp. 1020-1030, Mar. 2013.
[7] M. Charkhgard and M. Farrokhi, "State-of-charge estimation for lithium-ion batteries using neural networks and EKF," *IEEE Trans. Industrial Electron.*, Vol. 57, No. 12, pp. 4178-4187, Dec. 2010.
[8] M.-F. Tsai, Y.-Y. Peng, C.-S. Tseng, and N.-S. Li, "Modeling and estimation of state of charge for Lithium-Ion batteries using ANFIS architecture," in *Industrial Electronics (ISIE), 2012 IEEE International Symposium on*, pp. 863-868, 2012.
[9] C. Fleischer, W. Waag, Z. Bai, and D. U. Sauer, "Adaptive on-line state-of-available-power prediction of lithium-ion batteries," *Journal of Power Electronics*, Vol. 13, No. 4, pp. 516-527, Jul. 2013.
[10] Y. Zhao, H. Yun, S. Liu, H. Jiao, and C. Wang, "State-of-charge estimation for lithium-ion batteries using a multi-state closed-loop observer," *Journal of Power Electronics*, Vol. 14, No. 5, pp. 1038-1046, Sep. 2014.
[11] T. Kim, W. Qiao, and L. Qu, "Real-time state of charge and electrical impedance estimation for lithium-ion batteries based on a hybrid battery model," in *Applied Power Electronics Conference and Exposition (APEC), 2013 Twenty-Eighth Annual IEEE*, pp. 563-568, 2013.
[12] A. Vasebi, M. Partovibakhsh, and S. M. T. Bathaee, "A novel combined battery model for state-of-charge estimation in lead-acid batteries based on extended Kalman filter for hybrid electric vehicle applications," *Journal of Power Sources*, Vol. 174, No. 1, pp. 30-40, Nov. 2007.
[13] S. M. Rezvanizaniani, Z. Liu, Y. Chen, and J. Lee, "Review and recent advances in battery health monitoring and prognostics technologies for electric vehicle (EV) safety and mobility," *Journal of Power Sources*, Vol. 256, pp. 110-124, Jun. 2014.
[14] G. L. Plett, "Extended Kalman filtering for battery management systems of LiPB-based HEV battery packs: Part 1. Background," *Journal of Power Sources*, Vol. 134, No. 2, pp. 252-261, Aug. 2004.
[15] G. Welch and G. Bishop, "An introduction to the Kalman filter," University of North Carolina at Chapel Hill Chapel Hill, NC, USA, Technical Report1995
[16] G. L. Plett, "Extended Kalman filtering for battery management systems of LiPB-based HEV battery packs: Part 3. State and parameter estimation," *Journal of Power Sources*, Vol. 134, No. 2, pp. 277-292, Aug. 2004.
[17] W. Waag, S. Käbitz, and D. U. Sauer, "Experimental investigation of the lithium-ion battery impedance characteristic at various conditions and aging states and its influence on the application," *Applied Energy*, Vol. 102, pp. 885-897, Feb. 2013.
[18] X. Tang, X. Zhang, B. Koch, and D. Frisch, "Modeling and estimation of Nickel Metal Hydride battery hysteresis for SOC estimation," in *Prognostics and Health Management, 2008. PHM 2008. International Conference on*, pp. 1-12, 2008.
[19] H. R. Eichi and M.-Y. Chow, "Modeling and analysis of battery hysteresis effects," in *Energy Conversion Congress and Exposition (ECCE), 2012 IEEE*, pp. 4479-4486, 2012.
[20] H. L. N. Wiegman, "Battery state estimation and control for power buffering applications," Ph.D. dissertation, Dept. Elect. and Comp. Eng., Uni. of Wisconsin - Madison, 1999.
[21] M. A. Roscher and D. U. Sauer, "Dynamic electric behavior and open-circuit-voltage modeling of LiFePO4-based lithium ion secondary batteries," *Journal of Power Sources*, Vol. 196, No. 1, pp. 331-336, Jan. 2011.
[22] H. He, R. Xiong, X. Zhang, F. Sun, and J. Fan, "State-of-charge estimation of the lithium-ion battery using an adaptive extended Kalman filter based on an improved thevenin model," *IEEE Trans. Veh. Technol.*, Vol. 60, No. 4, pp. 1461-1469, May 2011.
[23] S. Lee, J. Kim, J. Lee, and B. H. Cho, "State-of-charge and capacity estimation of lithium-ion battery using a new open-circuit voltage versus state-of-charge," *Journal of Power Sources*, Vol. 185, No. 2, pp. 1367-1373, Dec. 2008.
[24] H. Dai, X. Wei, Z. Sun, J. Wang, and W. Gu, "Online cell SOC estimation of Li-ion battery packs using a dual time-scale Kalman filtering for EV applications," *Applied Energy*, Vol. 95, pp. 227-237, Mar. 2012.
[25] D. Kahaner, C. Moler, and S. Nash, *Numerical methods and software*, Prentice-Hall, Inc. Upper Saddle River, NJ, USA, 1989.
[26] M. Chen and G. A. Rincon-Mora, "Accurate electrical battery model capable of predicting runtime and I-V performance," *IEEE Trans. Energy Convers.*, Vol. 21, No. 2, pp. 504-511, Jun. 2006.
[27] L. Liao, P. Zuo, Y. Ma, X. Chen, Y. An, Y. Gao, and G. Yin, "Effects of temperature on charge/discharge behaviors of LiFePO4 cathode for Li-ion batteries," *Electrochimica Acta*, Vol. 60, pp. 269-273, Jan. 2012.
[28] J. Gomez, R. Nelson, E. E. Kalu, M. H. Weatherspoon, and J. P. Zheng, "Equivalent circuit model parameters of a high-power Li-ion battery: Thermal and state of charge effects," *Journal of Power Sources*, Vol. 196, No. 10, pp. 4826-4831, May 2011.
[29] T. Shuo, H. Munan, and O. Minggao, "An experimental study and nonlinear modeling of discharge behavior of valve-regulated lead acid batteries," *IEEE Trans. Energy Convers.*, Vol. 24, No. 2, pp. 452-458, Jun. 2009.
[30] J. Kim, S. Lee, and B. Cho, "Discharging/charging voltage-temperature pattern recognition for improved SOC/capacity estimation and SOH prediction at various temperatures," *Journal of Power Electronics*, Vol. 12, No. 1, pp. 1-9, Jan. 2012.

Van Huan Duong was born in Bac Giang, Vietnam, in 1985. He received his B.S. and M.S. degrees in Electrical Engineering from Hanoi University of Science and Technology, Vietnam, in 2008 and Soongsil University, Korea, in 2013, respectively. He is currently working toward his Ph.D. degree in Electrical Engineering at the University of

Wollongong, Australia. His current research interests include battery management system and microcontroller unit/digital signal processor applications.

Ngoc Tham Tran was born in Quang Nam, Vietnam, in 1987. He received his B.S. and M.S. degrees in Electrical Engineering from Danang University of Technology, Vietnam, in 2010 and Soongsil University, Republic of Korea in 2015, respectively. He is currently with the Department of Science and Technology, Danang University of Technology. His current research interests include battery management system for electric vehicles, such as battery modeling and state-of-charge and state-of-health estimation.

Woojin Choi was born in Seoul, Republic of Korea, in 1967. He received his B.S. and M.S. degrees in Electrical Engineering from Soongsil University, Republic of Korea, in 1990 and 1995, respectively, and his Ph.D. degree, also in Electrical Engineering, from Texas A&M University, USA, in 2004. From 1995 to 1998, he was with Daewoo Heavy Industries as a research engineer. In 2005, he joined the School of Electrical Engineering, Soongsil University. His research interests include modeling and controlling electrochemical energy sources, such as fuel cells, batteries, and supercapacitors; power conditioning technologies in renewable energy systems; and DC-DC converters for fuel cells and hybrid electric vehicles.

Dae-Wook Kim was born in Seoul, Republic of Korea, in 1973. He received his B.A. and Ph.D. degrees in Economics from Yonsei University, Republic of Korea, in 1999 and the University of California in Davis, USA, in 2004, respectively. From 2004 to 2007, he was with the Korea Institute for Industrial Economics and Trade as a research fellow. In 2007, he joined the Department of Economics, Soongsil University. His current interests include energy economics, particularly market structure and competition in energy industries.